Published in final edited form as:

Nat Cell Biol. 2017 January ; 19(1): 60–67. doi:10.1038/ncb3453.

LIN28 phosphorylation by MAPK/ERK couples signaling to the post-transcriptional control of pluripotency

Kaloyan M. Tsanov[1], **Daniel S. Pearson**[1], **Zhaoting Wu**[1], **Areum Han**[1], **Robinson Triboulet**[2], **Marc T. Seligson**[1], **John T. Powers**[1], **Jihan K. Osborne**[1], **Susan Kane**[3], **Steven P. Gygi**[4], **Richard I. Gregory**[2], and **George Q. Daley**[1,5]

[1]Stem Cell Transplantation Program, Division of Hematology/Oncology, Manton Center for Orphan Disease Research, Boston Children's Hospital and Dana Farber Cancer Institute; Department of Biological Chemistry and Molecular Pharmacology, Harvard Stem Cell Institute, Harvard Medical School; Howard Hughes Medical Institute, Boston, Massachusetts 02115, USA

[2]Stem Cell Program, Division of Hematology/Oncology, Boston Children's Hospital; Department of Biological Chemistry and Molecular Pharmacology, Harvard Stem Cell Institute, Harvard Medical School, Boston, Massachusetts 02115, USA

[3]Cell Signaling Technology, Inc., Danvers, Massachusetts 01923, USA

[4]Department of Cell Biology, Harvard Medical School, Boston, Massachusetts 02115, USA

Abstract

Signaling and post-transcriptional gene control are both critical for the regulation of pluripotency[1,2], yet how they are integrated to influence cell identity remains poorly understood. LIN28 (also known as LIN28A), a highly conserved RNA-binding protein (RBP), has emerged as a central post-transcriptional regulator of cell fate through blockade of *let-7* microRNA (miRNA) biogenesis and direct modulation of mRNA translation[3]. Here we show that LIN28 is phosphorylated by MAPK/ERK in pluripotent stem cells (PSCs), which increases its levels via post-translational stabilization. LIN28 phosphorylation had little impact on *let-7* but enhanced LIN28's effect on its direct mRNA targets, revealing a mechanism that uncouples LIN28's *let-7*-dependent and independent activities. We have linked this mechanism to the induction of pluripotency by somatic cell reprogramming and the transition from naïve to primed pluripotency. Collectively, our findings indicate that MAPK/ERK directly impacts LIN28, defining an axis that connects signaling, post-transcriptional gene control, and cell fate regulation.

[5]Correspondence should be addressed to G.Q.D. (george.daley@childrens.harvard.edu).

AUTHOR CONTRIBUTIONS

K.M.T. designed and performed the experiments, and wrote the manuscript. D.S.P. helped with RNA-seq, HeLa clonal series generation and expression analysis. Z.W. performed reprogramming experiments. A.H. performed RNA-seq bioinformatics analysis. R.T. and R.I.G. shared unpublished results and generated the isogenic HeLa cells. M.T.S. performed expression analysis. J.T.P. and J.K.O. helped with experimental design. S.K. generated the human pLIN28A antibody. S.P.G. supervised the proteomics experiments. G.Q.D. designed and supervised experiments, and wrote the manuscript.

COMPETING FINANCIAL INTERESTS

G.Q.D. and R.I.G. hold options and intellectual property related to 28/7 Therapeutics, a company seeking to develop inhibitors of the LIN28/*let-7* pathway. S.K. is an employee of Cell Signaling Technology.

The control of pluripotency requires precise coordination of multiple gene regulatory mechanisms, yet how this is orchestrated at the molecular level remains incompletely understood. Signaling has a key role in this network[1], with the MAPK/ERK pathway holding a particularly prominent place, since its activity primes PSCs for lineage commitment[4] whereas its inhibition is essential for the maintenance of a "naïve" state of pluripotency[5]. The effects of MAPK – and signaling pathways in general – are typically associated with downstream transcriptional mechanisms, while less is known about their integration with the post-transcriptional gene regulatory machinery[1,2]. Gaining insights into the latter is critical, as post-transcriptional mechanisms play a major role in the control of cell identity, especially in guiding transitions between cell fates[2].

LIN28, a highly conserved RBP, is a master post-transcriptional regulator of cell fate that controls embryonic development from *C. elegans* to mammals[3,6]. It supports the proliferative and metabolic capacities of PSCs, promotes reprogramming to pluripotency, and facilitates the transition from naïve to primed pluripotency[3,7–9]. Its effects are mediated through blockade of the biogenesis of the *let-7* miRNA family[10–13], and through direct translational enhancement or suppression of select mRNAs[9,14–18].

To gain insight into how LIN28 is integrated with the pluripotency signaling network, we investigated the role of LIN28 phosphorylation. Global phosphoproteomic studies of human embryonic stem cells (hESCs) had identified several putative phosphosites in LIN28[19,20]. To validate their conservation between human and mouse, we employed a targeted phosphoproteomics strategy in mouse ESCs (mESCs) (Supplementary Fig. 1a–c). We were able to map four phosphosites, two of which, S184 and S200, were confidently assigned to specific serine residues (Supplementary Table 1). Combining our data and prior results[19,20], we generated a comprehensive profile of LIN28 phosphorylation in PSCs (Fig. 1a).

To identify kinases that phosphorylate LIN28, we interrogated the LIN28 amino acid sequence for conserved kinase recognition motifs (Supplementary Fig. 1d). Since we noticed members of the MAPK family as predicted kinases for S200, we decided to further investigate this phosphorylation event (Fig. 1b). We generated an antibody reactive against phospho-S200 and validated its specificity with a phospho-null LIN28 mutant, in which S200 is mutated to alanine (S200A) (Fig. 1c). Using this antibody, we profiled a panel of human PSCs, all of which exhibited LIN28 (S200) phosphorylation, suggesting that the latter is a common molecular feature of PSCs (Supplementary Fig. 1e).

To identify the particular MAPK responsible for S200 phosphorylation, we performed a targeted inhibitor screen in human embryonal carcinoma cells (hECCs). We used selective inhibitors of the major MAPKs, including MEK/ERK, p38 MAPK, JNKs, CDKs, and GSK3β, as well as mTOR, an unrelated proline-directed kinase. Of those, only the MEK/ERK inhibitor, PD0325901, consistently reduced S200 phosphorylation under the tested conditions (Fig. 1d). We then serum-starved hECCs and subjected them to short-term treatment with phorbol myristate acetate (PMA), which activates MAPK/ERK signaling. S200 phosphorylation was induced, corroborating the inhibitor data (Fig. 1e). Pre-treatment with the MEK/ERK inhibitor but not with an inhibitor of a different MAPK, p38 MAPK,

abrogated the PMA-induced phosphorylation of LIN28, indicating that the PMA effects are mediated via ERK (Fig. 1e).

To confirm this conclusion, we also expressed wild-type, constitutively active (R4F), or kinase-dead (K97M) versions of MEK1[21] in 293T cells stably expressing a LIN28 ORF and subjected them to serum starvation. As expected, only the R4F mutant was able to activate ERK and maintain LIN28 phosphorylation under these conditions (Fig. 1f). Lastly, we serum-starved hECCs and added back serum or treated them with fibroblast growth factor (FGF) or epidermal growth factor (EGF), physiologically relevant cues that induce ERK signaling. All three treatments led to increased LIN28 phosphorylation (Fig. 1g). Collectively, our results demonstrate that ERK phosphorylates LIN28 on S200 in response to mitogenic stimuli.

Next, we explored whether S200 phosphorylation affects LIN28 function. Intriguingly, we noticed that pre-treatment with the phosphatase inhibitor Calyculin A led to increased LIN28 abundance in our mass spectrometry samples (Supplementary Fig. 1b). Western blot analysis confirmed an approximately 30% increase of LIN28 protein (Fig. 2a). A similar effect was observed in the MEK1 overexpression experiments (Fig. 1f), suggesting that ERK-mediated phosphorylation may stabilize LIN28 protein. To test this hypothesis, we treated hECCs with PMA for three hours, which led to a 30% increase in LIN28 protein, without concordant mRNA changes (Fig. 2b). Conversely, a 48-hour treatment with the MEK/ERK inhibitor resulted in a one-third decrease of LIN28 at the protein but not mRNA level (Fig. 2c and Supplementary Fig. 2a), overall supporting our hypothesis.

To further explore this question, we generated stable isogenic 293T and HeLa cell lines expressing wild-type, phospho-mimetic (S200D or S200E), or phospho-null (S200A) LIN28, in which serine phosphorylation is mimicked or abrogated by substitution with aspartate/glutamate or alanine, respectively. While the phospho-mimetics showed 50–100% increase in protein levels, the phospho-null exhibited 40–50% decrease, without corresponding mRNA changes (Fig. 2d). These data indicate that the observed effects on LIN28's protein levels are post-translational and specifically mediated through the ERK target site in LIN28.

Lastly, we performed cycloheximide chase experiments in hECCs to track the decay kinetics of endogenous pLIN28 (S200) and total LIN28. While the total protein decayed with an estimated half-life of 12 hours, the phosphoprotein remained stable for the 24-hour course of the experiment (after an initial treatment-induced phosphorylation spike), suggesting that pLIN28 has a longer half-life and is thus relatively more stable (Fig. 2e). We then conducted analogous experiments using the isogenic HeLa cells expressing LIN28 phosphorylation mutants, which showed that the mimetic (S200E) and null (S200A) mutants decay slower and faster, respectively, compared to wild-type LIN28 (Fig. 2f). As these LIN28 variants are under doxycycline-control, we also withdrew doxycycline and tracked their decay kinetics in an unperturbed way, which confirmed the cycloheximide chase results (Fig. 2g). Taken together, the above data indicate that ERK-mediated phosphorylation stabilizes LIN28 post-translationally by increasing its protein half-life.

We then examined the effect of LIN28 phosphorylation on its downstream targets. First, we assessed *let-7* regulation. We performed *let-7* measurements in hECCs after a 48-hour treatment with the MEK/ERK inhibitor, which revealed a lack of statistically significant change in *let-7* levels (Supplementary Fig. 2b). These data suggested that the ~30% reduction of LIN28 abundance due to loss of phosphorylation was insufficient to consistently affect *let-7* processing. In support of this observation, ~30% knockdown of LIN28 protein yielded similar results (Supplementary Fig. 3a). To further address this question, we derived individual clones of HeLa cells stably expressing wild-type LIN28 at different levels. LIN28 protein expression equivalent to about 50% of its native level in hECCs achieved saturation of *let-7* suppression, confirming our earlier conclusion (Supplementary Fig. 4a). To specifically assess the role of S200 phosphorylation, we also measured *let-7* levels in the isogenic HeLa cells expressing wild-type or phospho-null (S200A) LIN28. As expected, the two LIN28 variants achieved comparable *let-7* suppression despite the consistently lower protein levels of the S200A mutant (Supplementary Fig. 4b,c).

We then performed RNA immunoprecipitation (RIP) experiments in hECCs stably overexpressing wild-type or phospho-mimetic (S200D) LIN28 (Fig. 3a), followed by qRT-PCR measurement of pri/pre-*let-7* association. The two proteins precipitated comparable amounts of most pri/pre-*let-7*s analyzed, consistent with lack of effect on *let-7* processing (Fig. 3b). In line with these results, mature *let-7* levels were also unchanged in the mimetic relative to the wild-type cells (Fig. 3c). Overall, our data from multiple assays demonstrate that LIN28 phosphorylation does not have a significant impact on *let-7*.

Next, we explored the effect of LIN28 phosphorylation on its mRNA targets. To do this on a transcriptome-wide scale, we performed RNA immunoprecipitation coupled with mRNA-seq (RIP-seq) of the wild-type and phospho-mimetic (S200D) LIN28 in hECCs. When normalized to the amount of immunoprecipitated LIN28, the two proteins showed highly similar mRNA binding profiles, indicating that they have comparable affinities to their mRNA targets (Fig. 3d). However, when normalized to cell number, a follow-up qRT-PCR analysis of representative mRNAs revealed a stoichiometric increase in mRNA association that was specific to the LIN28 targets (Fig. 3e). Of note, similar results were obtained with the S200E mutant in the isogenic HeLa cells (Supplementary Fig. 4f,g). Overall, these data suggest that the phospho-mimetic mutants have comparable mRNA binding affinities to the wild-type protein but, due to their higher abundance per cell, associate with a greater amount of the same targets.

To further support this conclusion, we also performed complementary analysis in the isogenic HeLa cells expressing wild-type or phospho-null (S200A) LIN28. Consistent with its reduced protein abundance, the phospho-null LIN28 reproducibly precipitated lower amount of RNA per cell relative to the wild-type construct, which was proportional to their respective protein levels (Supplementary Fig. 4d). However, when normalized to the amount of immunoprecipitated LIN28, the two constructs showed aligned mRNA binding profiles, corroborating the hECC data (Supplementary Fig. 4e).

Lastly, we wanted to confirm that the changes in mRNA binding per cell affect their cognate protein expression, as LIN28 is known to modulate mRNA translation[9,14–18]. We validated a set of previously established LIN28 mRNA targets by assessing their mRNA and protein levels after ~30% LIN28 knockdown in hECCs. As expected, mRNA levels were unaffected while protein levels decreased (for RPS13) or increased (for RPL23, NDUFB3, NDUFB8, and NDUFB10), in agreement with their reported LIN28-dependent translational enhancement and suppression, respectively (Supplementary Fig. 3b,c)[9,14,15]. We then performed qRT-PCR and Western blot analyses of these targets in the hECCs expressing wild-type or phospho-mimetic (S200D) LIN28. While the mRNA levels were unchanged, protein levels were altered in the mimetic relative to the wild-type construct, consistent with stronger translational activity of LIN28 (Fig. 3f,g). Importantly, these protein changes were in the opposite direction to the ones observed after LIN28 depletion and involved both positively and negatively regulated targets, suggesting that they reflect LIN28's overall translational activity rather than only its translation-promoting or suppressing function. Together, our results indicate that ERK-mediated LIN28 phosphorylation has little impact on *let-7* but enhances LIN28's regulation of its mRNA targets, thereby acting as a mechanism for uncoupling of LIN28's *let-7*-dependent and independent activities.

Given these molecular findings, we wondered if this mechanism regulates LIN28's function in guiding cell fate transitions. As LIN28 potently promotes the induction of pluripotency via somatic cell reprogramming[7], we performed factor-based reprogramming using wild-type, phospho-null (S200A), or phospho-mimetic (S200D) LIN28 in combination with OCT4, SOX2 and NANOG. Consistent with our earlier data, the S200A and S200D mutants showed lower and higher protein expression than the wild-type, respectively, without concordant mRNA changes (Fig. 4a). The altered LIN28 protein abundance further appeared insufficient to differentially affect *let-7* (Fig. 4b). Importantly, however, the S200A and S200D LIN28 led to approximately 50% decreased or increased reprogramming efficiency, respectively, indicating that S200 phosphorylation and its effect on LIN28 have a substantial role in the induction of pluripotency (Fig. 4c).

We then addressed LIN28's function in ESCs. Since ERK[5] and LIN28[8,9] control the transition from naïve to primed pluripotency, we explored the regulation of LIN28 levels in mESCs cultured in serum/LIF versus dual-inhibitor/LIF (2i/LIF) conditions. Consistent with previous reports[8,9], LIN28 levels were reduced both at the protein and mRNA level in the 2i/LIF culture (Fig. 4d). To examine whether ERK-dependent post-translational control contributes to this reduction, we performed inhibitor dropout experiments. Short-term removal of the MEK/ERK inhibitor – but not the GSK3β inhibitor – led to a ~30% increase in LIN28 protein but not mRNA, supporting an ERK-mediated protein stabilization model (Fig. 4e). To confirm that S200 phosphorylation is involved, we replaced endogenous LIN28 with wild-type, phospho-mimetic (S200D), or phospho-null (S200A) LIN28 by expressing respective ORF constructs into mESCs with knocked out LIN28A/B loci. Consistent with our earlier data, the mimetic and null maintained higher and lower protein levels (when cultured in serum), respectively, without analogous mRNA changes (Fig. 4f). We then performed clonogenic assays upon transfer from 2i/LIF to serum/LIF and assessed the alkaline phosphatase (AP) staining pattern of colonies emerging in the serum/LIF culture, which is characterized by a mix of compact, uniformly AP-positive, naïve-like ("solid")

colonies and larger, heterogeneously AP-stained, more primed ("mixed") colonies[8]. The S200D mutant showed a reproducibly lower fraction of solid colonies while the S200A exhibited a higher fraction relative to wild-type LIN28, demonstrating that the higher LIN28 protein level mediated by S200 phosphorylation enhances LIN28's function in promoting the transition from naïve to primed pluripotency (Fig. 4g). Together, our reprogramming and ESC data demonstrate that LIN28 phosphorylation contributes to the regulation of pluripotency transitions.

In sum, our results indicate that LIN28 phosphorylation by MAPK/ERK serves as a molecular link between signaling, post-transcriptional gene regulation, and cell fate control. While ERK is known to impact numerous pluripotency transcription factors[22], LIN28 is an RBP and thus represents a distinct mechanism by which ERK signaling regulates gene expression and cell identity. Of note, ERK has also been suggested to regulate LIN28 transcriptionally[8,23], so it may exert dual regulation on LIN28 to ensure timely and robust control of LIN28 levels. Given the repertoire of pluripotency-associated RBPs[24] and a recent link between ERK and the RBP Brf1 in mESCs[25], other RBPs may be similarly regulated by ERK to modulate cell fate.

Adding to prior findings[8,9], the ERK-LIN28 coupling reported here further implicates LIN28 as a "priming" factor and suggests that its activity is particularly relevant in guiding transitions between cell states, closely matching its primordial function in *C. elegans*[6]. Given the critical role of timing for these transitions, post-translational mechanisms are well-suited to control LIN28 function. As we and others have mapped multiple phosphorylation sites on LIN28 (Fig. 1a), additional kinase pathways may also regulate LIN28. Other post-translational modifications, namely acetylation[26] and methylation[27], have also been reported to control LIN28, so the latter appears to integrate both extrinsic and intrinsic signals, in line with its role as a key hub of post-transcriptional gene regulation.

Finally, the mechanism described herein highlights the role of LIN28's *let-7*-independent activities in cell fate regulation and may also explain the intriguing observation that LIN28's *let-7*-independent functions precede its *let-7*-mediated ones during cell differentiation and organismal development[28,29]. A gradual, controlled decrease in LIN28 levels, initiated by protein destabilization, may allow for disengagement of its mRNA targets prior to effects on *let-7*.

METHODS

Plasmids

For stable expression, FLAG-LIN28A was subcloned in the pBabe-Puro (retroviral) or pSin-Puro (lentiviral) vectors. pBabe-Puro was a gift from H. Land, J. Morgenstern, and R. Weinberg (Addgene plasmid #1764)[30], and pSin was a gift from J. Thomson (Addgene plasmid #16578)[7]. Phospho-mimetic and phospho-null mutants were generated using the QuikChange Lightning site-directed mutagenesis kit (Agilent Technologies), as per manufacturer's protocol. pMCL-HA-MEK1 wild-type, constitutively active (R4F), and kinase-dead (K97M) plasmids were gifts from N. Ahn (Addgene plasmids #48808, 40810, 40811)[21].

Cell Culture

iLIN28A[31], v6.5[32], and LIN28A/B KO[33] mESCs were maintained on irradiated CF1 MEFs (GlobalStem) in mESC medium (DMEM, 15% FBS, 1 U/ml Penicillin, 1 μg/ml Streptomycin, 2 mM L-glutamine, 0.1 mM NEAA, 0.1 mM BME, 1,000 U/ml LIF). hESCs (CHB6, NIH#0006), MSC-iPSCs[34], and BJ1-iPSCs[34] were maintained in hESC medium (DMEM/F12, 20% KOSR, 1 U/ml Penicillin, 1 μg/ml Streptomycin, 2 mM L-glutamine, 0.1 mM NEAA, 0.1 mM BME, 4 ng/ml FGF). PA1 (ATCC# CRL-1572), NCCIT (ATCC# CRL-2073), HeLa (ATCC# CCL-2), and 293T cells were maintained in DMEM/10% FBS. 293T(RMCE) cells were a gift from E. Makeyev; LIN28-expressing lines were generated following published protocols[35]. HeLa Flp-In cell lines were generated as described previously[36]. 2i/LIF culture was performed following published protocols[5]. No cell lines used in this study were found in the database of commonly misidentified cell lines that is maintained by ICLAC and NCBI Biosample. The cell lines were not authenticated. The cell lines were tested mycoplasma-negative.

Transfections

For plasmid transfections, 293T cells were seeded at 4×10^5 cells/well in 6-well plates, transfected with 2 ug respective plasmid 16–20 hours later using X-tremeGENE 9 (Roche), and analyzed after another 48 hours. For siRNA transfections, PA1 cells were seeded at 3×10^5 cells/well in 6-well plates, transfected with 0.25 pmol siRNA 16–20 hours later using Lipofectamine RNAiMAX (Invitrogen), and harvested by trypsinization after another 96 hours. The following siRNAs were used: siNC (Ambion #4390843); siLIN28A (Ambion #4392420-s36195).

Viral Production and Stable Cell Line Generation

Viral production was carried out as described previously[9]. Transgenic PA1 and HeLa cells were generated by transduction with unconcentrated viral supernatant and selection with 1 ug/ml Puromycin. HeLa-LIN28A clones were derived by isolation and expansion of single cells from a heterogeneous pool of stable transductants. For transgenic mESC generation, lentivirus was concentrated using the Lenti-X Concentrator (Clontech) and used for transduction in 2i/LIF medium, followed by selection with 1 ug/ml Puromycin.

Drug Treatments

Drugs used were: Calyculin A (Cell Signaling), Torin1 (Tocris), PD0325901 (Stemgent), SB203580 (Invivogen), SP600125 (Sigma), Kenpaullone (Sigma), LY294002 (Cell Signaling), bFGF (Gemini), EGF (Peprotech), PMA (Cell Signaling), CHX (Sigma), and Doxycycline (Sigma). Treatment conditions are described in detail in the text.

Affinity Purification

For mass spectrometry analysis, iLIN28A mESCs were treated with: (i) 1 μg/ml Doxycycline (Sigma) for 48 hours to induce FLAG-LIN28A expression, and (ii) 100 nM Calyculin A (Cell Signaling) for 30 minutes immediately prior to harvest to enrich for phosphorylation events. Cells were harvested in cold PBS and immediately lysed in M2 lysis buffer (50 mM Tris-HCl pH 7.5, 150 mM NaCl, 1 mM EDTA, 1% Triton X-100) containing

2X protease and phosphatase inhibitors (Pierce). FLAG-tagged LIN28 variants were purified using the anti-FLAG M2 affinity gel following the manufacturer's specifications (Sigma).

Mass Spectrometry

Affinity purified proteins were separated on a 4–20% polyacrylamide gel (Bio-Rad) and visualized using the Bio-Safe Coomassie Stain (Bio-Rad). The band containing FLAG-LIN28A was excised and treated with dithiotriethol to reduce disulfide bonds and iodoacetamide to alkylate cysteines. In-gel digestion of the protein was performed with trypsin or chymotrypsin. The resulting peptides were extracted from the gel and analyzed by liquid chromatography tandem mass spectrometry (LC-MS/MS), as described previously[37]. All peptide matches were filtered based on mass accuracy, tryptic state (for trypsin), and XCorr, and confirmed by manual inspection. The reliability of site-localization of phosphorylation events was evaluated using the Ascore algorithm[38].

Antibody Generation

Human and mouse-reactive pLIN28(S200) rabbit polyclonal antibodies were produced by immunizing animals with a synthetic phosphopeptide corresponding to residues surrounding S200 of human or mouse LIN28A, respectively. Antibodies were purified by protein A and peptide affinity chromatography. The human-reactive antibody was generated by Cell Signaling (Danvers, MA) and the mouse-reactive antibody by GenScript (Piscataway, NJ).

Western Blot

Cells were lysed in RIPA buffer containing protease and phosphatase inhibitors (Pierce). Proteins were separated on a 4–20% polyacrylamide gel (Bio-Rad) and transferred to a methanol-activated PVDF membrane (Millipore). The membrane was blocked for 30–60 minutes in 3%BSA/PBST (chemiluminescent blots) or 3%BSA/PBS (fluorescent blots), and probed with primary antibodies at 4°C overnight. Secondary antibody incubation was performed at room temperature for 1–2 hours. Protein levels were detected using the SuperSignal West Pico and Femto Luminol reagents (Thermo Scientific) or the Odyssey CLx near-infrared fluorescence imaging system (LI-COR). Primary antibodies used were: anti-pLIN28(S200) (generated as described above; 1:1,000), anti-LIN28A (Cell Signaling #3978; 1:1,000), anti-α/β-tubulin (Cell Signaling #2148; 1:1,000), anti-pERK1/2 (Sigma E7028; 1:1,000), anti-ERK1/2 (Cell Signaling #4695, clone 137F5; 1:1,000), anti-FLAG (Sigma F3165, clone M2; 1:1,000), anti-Actin (Santa Cruz sc-1616; 1:2,000), anti-HA (Sigma H6533, clone HA-7; 1:1,000), anti-RPS13 (Abcam ab104862; 1:1,000), anti-RPL23 (Proteintech #16086-1-AP; 1:1,000), anti-NDUFB3 (Abcam ab55526; 1:1,000), anti-NDUFB8 (Abcam ab110242, clone 20E9DH10C12; 1:1,000), anti-NDUFB10 (Proteintech #15589-1-AP; 1:1,000). Secondary antibodies used were: for chemiluminescence, HRP-conjugated anti-rabbit IgG (GE Healthcare NA934, 1:2,000), anti-mouse IgG (GE Healthcare NA931; 1:2,000), and anti-goat IgG (Santa Cruz sc-2020; 1:2,000); for fluorescence, IRDye 680RD anti-rabbit IgG (LI-COR #925-68071; 1:20,000), IRDye 800CW anti-mouse IgG (LI-COR #925-32210; 1:20,000), and IRDye 680RD anti-goat IgG (LI-COR #925-68074; 1:20,000). Quantifications were performed using ImageJ (chemiluminescent blots) or Image Studio for Odyssey CLx (fluorescent blots) (LI-COR).

Quantitative RT-PCR

Total RNA was isolated using Trizol (Invitrogen) combined with miRNeasy columns (Qiagen). 100–250 ng RNA were reverse-transcribed using the miScript II RT kit (Qiagen) and subjected to miScript miRNA assays (Qiagen) or standard mRNA assays. miRNA and mRNA expression was measured by SYBR Green quantitative PCR using the ΔΔCt method. U6 and β-actin were used for normalization of miRNA and mRNA measurements, respectively. Primers used were: hLIN28A (F: GAGCATGCAGAAGCGCAGATCAAA; R: TATGGCTGATGCTCTGGCAGAAGT); FLAG-hLIN28A (F: ATGACGACAAGGGCTCCG; R: CGCACGTTGAACCACTTACA); hACTB (F: AGAAGGATTCCTATGTGGGCG; R: CATGTCGTCCCAGTTGGTGAC); mLin28a (F: AGGCGGTGGAGTTCACCTTTAAGA; R: AGCTTGCATTCCTTGGCATGATGG); mActB (F: CAGAAGGAGATTACTGCTCTGGCT; R: TACTCCTGCTTGCTGATCCACATC); hRPS13 (F: TCCCAGTCGGCTTTACCCTAT; R: CAGGATTACACCGATCTGTGAAG); hRPL23 (F: TCCTCTGGTGCGAAATTCCG; R: CGTCCCTTGATCCCCTTCAC); hNDUFB3 (F: GCTGGCTGCAAAAGGGCTA; R: CTCCTACAGCTACCACAAATGC); hNDUFB8 (F: CCGCCAAGAAGTATAATATGCGT; R: TATCCACACGGTTCCTGTTGT); hNDUFB10 (F: AGCCCAATCCCATCGTCTACA; R: GCTGCCGCTCTATAAATTCTCT); pri/pre-let-7a (F: TGAGGTAGTAGGTTGTATAGTTTTAGGG; R: GGAAAGACAGTAGATTGTATAGTTATC); pri/pre-let-7b (Qiagen #MP00000028); pri/pre-let-7c (Qiagen #MP00000035); pri/pre-let-7d (Qiagen #MP00000042); pri/pre-let-7e (Qiagen #MP00000049); pri/pre-let-7g (Qiagen #MP00000070); pri/pre-let-7i (Qiagen #MP00000077); let-7a (Qiagen #MS00032179); let-7b (Qiagen #MS00001225); let-7c (Qiagen #MS00005852); let-7d (Qiagen #MS00001232); let-7e (Qiagen #MS00032186); let-7f (Qiagen #MS00005866); let-7g (Qiagen #MS00010983); let-7i (Qiagen #MS00001253); U6 (Qiagen #MS00033740).

RNA Immunoprecipitation

FLAG-tagged LIN28A variants were purified using the protocol described earlier, with the following modifications: (i) Calyculin A was omitted; (ii) 100 U/ml RNasin (Promega) was included in the lysis and wash buffers; (iii) RNA was isolated from the beads by resuspension in Trizol (Invitrogen). Parental PA1 or HeLa Flp-In cells (no FLAG) were used as controls for antibody specificity. RNA purification and qRT-PCR were performed as described earlier. The ΔΔCt method was used to calculate enrichment, whereby RIP Ct values were normalized to the corresponding input and no-FLAG control Ct values. RNA-seq was performed as described below.

RNA Sequencing

RNA >200 nt was isolated using Trizol (Invitrogen) combined with RNeasy columns (Qiagen). 50 ng purified RNA was subjected to polyA selection using the NEBNext Poly(A) mRNA Magnetic Isolation Module (NEB) and subsequently used for library preparation with the NEBNext Ultra RNA Library Prep Kit (NEB). Libraries were analyzed on a Bioanalyzer (Agilent) for quality control, quantified using the Qubit dsDNA HS Assay (Invitrogen) and qRT-PCR (Kapa Biosystems), and equimolar pools were sequenced on

HiSeq 2500 or NextSeq 500 instruments (Illumina) using 50-bp or 76-bp single-end protocols, respectively. Expression values (RPKM) were estimated using the TopHat[39] and HTSeq-count tools[40], and lowly expressed genes (RPKM ≤10) were filtered out. Enrichment scores for each gene were calculated by dividing the RPKM value of the target protein RIP by the RPKM value of the no-FLAG control RIP after normalization of each RIP value to its respective input value.

Reprogramming

Reprogramming assays were performed essentially as described previously[9]. Briefly, dH1f fibroblasts were seeded at 2.5×10^5 cells/well in a 12-well plate and transduced overnight with a pool of lentiviral (OCT4, SOX2, NANOG) and retroviral (LIN28A variants) particles. Six days later, cells were trypsinized and $1–2 \times 10^5$ cells/well were re-plated onto MEF-coated 12-well plates. Medium was switched to hESC medium and changed daily until day 21 when reprogramming efficiency was measured. To do so, cells were fixed with 4% paraformaldehyde and stained with biotin-anti-TRA-1-60 (eBioscience #13-8863-82; 1:250) and streptavidin-HRP (Biolegend #405210; 1:500) primary and secondary antibodies, respectively. Staining was developed with the DAB Peroxidase kit (Vector Labs), and the number of iPSC colonies was quantified using ImageJ. Experiments were carried out and analyzed in a blinded manner.

Clonal Assay

mESCs maintained in 2i/LIF were seeded on MEF-coated 6-well plates at clonal density (500 cells/well) and allowed to grow for 5 days. At this point, cells were stained using the Leukocyte Alkaline Phosphatase kit (Sigma) and classified as showing either solid or mixed alkaline phosphatase staining by visual inspection, as described previously[8].

Statistics and Reproducibility

All experiments were performed at least three independent times (unless noted otherwise) and respective data used for statistical analyses. Differences between groups were assessed using a two-tailed Student's *t*-test in Microsoft Excel, with data assumed to fulfill *t*-test requirements. For RIP-seq analysis, differences were assessed using paired *t*-tests and the Benjamini-Hochberg correction for multiple hypotheses testing. Statistical significance is displayed as $P<0.05$ (one asterisk) or $P<0.01$ (two asterisks). Error bars indicate s.e.m. Sample sizes and reproducibility for each experiment are described in the respective figure legends, and raw data from independent replicates are provided in Supplementary Table 4.

Data Availability

RNA-sequencing data that support the findings of this study have been deposited in the Gene Expression Omnibus (GEO) under accession code GSE83906. Proteomics data have been deposited in the Mass spectrometry Interactive Virtual Environment (MassIVE) under ID# MSV000080302. All other data supporting the findings of this study are available from the corresponding author upon reasonable request.

Supplementary Material

Refer to Web version on PubMed Central for supplementary material.

Acknowledgments

We thank P. Sharp, L. Cantley, G. Ruvkun, and members of the Daley lab for invaluable discussions, A. De Los Angeles for critical feedback on the manuscript, X. Wu/Yi Zhang's lab and R. Rubio/DFCI CCCB for assistance with RNA-seq, and R. Tomaino at the Taplin Biological Mass Spectrometry Core for assistance with mass spectrometry. Bioanalyzer analysis was performed in the BCH IDDRC Molecular Genetics Core, which is supported by NIH (NIH-P30-HD 18655). Sequencing analysis was conducted on the Orchestra High Performance Computing Cluster at Harvard Medical School. K.M.T. was an HHMI International Student Research Fellow and a Herchel Smith Graduate Fellow. D.S.P. was supported by a grant from NIGMS (T32GM007753). R.I.G was supported by a grant from NIGMS (R01GM086386). G.Q.D. is an investigator of the Howard Hughes Medical Institute and the Manton Center for Orphan Disease Research, and was supported by a grant from NIGMS (R01GM107536).

REFERENCES

1. Ng HH, Surani MA. The transcriptional and signalling networks of pluripotency. Nat Cell Biol. 2011; 13:490–496. [PubMed: 21540844]
2. Ye J, Blelloch R. Regulation of pluripotency by RNA binding proteins. Cell Stem Cell. 2014; 15:271–280. [PubMed: 25192462]
3. Shyh-Chang N, Daley GQ. Lin28: primal regulator of growth and metabolism in stem cells. Cell Stem Cell. 2013; 12:395–406. [PubMed: 23561442]
4. Kunath T, et al. FGF stimulation of the Erk1/2 signalling cascade triggers transition of pluripotent embryonic stem cells from self-renewal to lineage commitment. Development. 2007; 134:2895–2902. [PubMed: 17660198]
5. Ying QL, et al. The ground state of embryonic stem cell self-renewal. Nature. 2008; 453:519–523. [PubMed: 18497825]
6. Moss EG, Lee RC, Ambros V. The cold shock domain protein LIN-28 controls developmental timing in C. elegans and is regulated by the lin-4 RNA. Cell. 1997; 88:637–646. [PubMed: 9054503]
7. Yu J, et al. Induced pluripotent stem cell lines derived from human somatic cells. Science. 2007; 318:1917–1920. [PubMed: 18029452]
8. Kumar RM, et al. Deconstructing transcriptional heterogeneity in pluripotent stem cells. Nature. 2014; 516:56–61. [PubMed: 25471879]
9. Zhang J, et al. LIN28 Regulates Stem Cell Metabolism and Conversion to Primed Pluripotency. Cell Stem Cell. 2016
10. Heo I, et al. Lin28 mediates the terminal uridylation of let-7 precursor MicroRNA. Mol Cell. 2008; 32:276–284. [PubMed: 18951094]
11. Newman MA, Thomson JM, Hammond SM. Lin-28 interaction with the Let-7 precursor loop mediates regulated microRNA processing. RNA. 2008; 14:1539–1549. [PubMed: 18566191]
12. Rybak A, et al. A feedback loop comprising lin-28 and let-7 controls pre-let-7 maturation during neural stem-cell commitment. Nat Cell Biol. 2008; 10:987–993. [PubMed: 18604195]
13. Viswanathan SR, Daley GQ, Gregory RI. Selective blockade of microRNA processing by Lin28. Science. 2008; 320:97–100. [PubMed: 18292307]
14. Cho J, et al. LIN28A is a suppressor of ER-associated translation in embryonic stem cells. Cell. 2012; 151:765–777. [PubMed: 23102813]
15. Peng S, et al. Genome-wide studies reveal that Lin28 enhances the translation of genes important for growth and survival of human embryonic stem cells. Stem Cells. 2011; 29:496–504. [PubMed: 21425412]
16. Polesskaya A, et al. Lin-28 binds IGF-2 mRNA and participates in skeletal myogenesis by increasing translation efficiency. Genes Dev. 2007; 21:1125–1138. [PubMed: 17473174]

17. Shyh-Chang N, et al. Lin28 enhances tissue repair by reprogramming cellular metabolism. Cell. 2013; 155:778–792. [PubMed: 24209617]
18. Wilbert ML, et al. LIN28 binds messenger RNAs at GGAGA motifs and regulates splicing factor abundance. Mol Cell. 2012; 48:195–206. [PubMed: 22959275]
19. Rigbolt KT, et al. System-wide temporal characterization of the proteome and phosphoproteome of human embryonic stem cell differentiation. Sci Signal. 2011; 4:rs3. [PubMed: 21406692]
20. Van Hoof D, et al. Phosphorylation dynamics during early differentiation of human embryonic stem cells. Cell Stem Cell. 2009; 5:214–226. [PubMed: 19664995]
21. Mansour SJ, et al. Transformation of mammalian cells by constitutively active MAP kinase kinase. Science. 1994; 265:966–970. [PubMed: 8052857]
22. Cai N, Li M, Qu J, Liu GH, Izpisua Belmonte JC. Post-translational modulation of pluripotency. J Mol Cell Biol. 2012; 4:262–265. [PubMed: 22679102]
23. Dangi-Garimella S, et al. Raf kinase inhibitory protein suppresses a metastasis signalling cascade involving LIN28 and let-7. EMBO J. 2009; 28:347–358. [PubMed: 19153603]
24. Kwon SC, et al. The RNA-binding protein repertoire of embryonic stem cells. Nat Struct Mol Biol. 2013; 20:1122–1130. [PubMed: 23912277]
25. Tan FE, Elowitz MB. Brf1 posttranscriptionally regulates pluripotency and differentiation responses downstream of Erk MAP kinase. Proc Natl Acad Sci U S A. 2014; 111:E1740–E1748. [PubMed: 24733888]
26. Wang LX, Wang J, Qu TT, Zhang Y, Shen YF. Reversible acetylation of Lin28 mediated by PCAF and SIRT1. Biochim Biophys Acta. 2014; 1843:1188–1195. [PubMed: 24631505]
27. Kim SK, et al. SET7/9 methylation of the pluripotency factor LIN28A is a nucleolar localization mechanism that blocks let-7 biogenesis in human ESCs. Cell Stem Cell. 2014; 15:735–749. [PubMed: 25479749]
28. Balzer E, Heine C, Jiang Q, Lee VM, Moss EG. LIN28 alters cell fate succession and acts independently of the let-7 microRNA during neurogliogenesis in vitro. Development. 2010; 137:891–900. [PubMed: 20179095]
29. Vadla B, Kemper K, Alaimo J, Heine C, Moss EG. lin-28 controls the succession of cell fate choices via two distinct activities. PLoS Genet. 2012; 8:e1002588. [PubMed: 22457637]
30. Morgenstern JP, Land H. Advanced mammalian gene transfer: high titre retroviral vectors with multiple drug selection markers and a complementary helper-free packaging cell line. Nucleic Acids Res. 1990; 18:3587–3596. [PubMed: 2194165]
31. Zhu H, et al. Lin28a transgenic mice manifest size and puberty phenotypes identified in human genetic association studies. Nat Genet. 2010; 42:626–630. [PubMed: 20512147]
32. Eggan K, et al. Hybrid vigor, fetal overgrowth, and viability of mice derived by nuclear cloning and tetraploid embryo complementation. Proc Natl Acad Sci U S A. 2001; 98:6209–6214. [PubMed: 11331774]
33. Shinoda G, et al. Fetal deficiency of lin28 programs life-long aberrations in growth and glucose metabolism. Stem Cells. 2013; 31:1563–1573. [PubMed: 23666760]
34. Park IH, et al. Reprogramming of human somatic cells to pluripotency with defined factors. Nature. 2008; 451:141–146. [PubMed: 18157115]
35. Khandelia P, Yap K, Makeyev EV. Streamlined platform for short hairpin RNA interference and transgenesis in cultured mammalian cells. Proc Natl Acad Sci U S A. 2011; 108:12799–12804. [PubMed: 21768390]
36. Triboulet R, Pirouz M, Gregory RI. A Single Let-7 MicroRNA Bypasses LIN28-Mediated Repression. Cell Rep. 2015; 13:260–266. [PubMed: 26440890]
37. Villen J, Gygi SP. The SCX/IMAC enrichment approach for global phosphorylation analysis by mass spectrometry. Nat Protoc. 2008; 3:1630–1638. [PubMed: 18833199]
38. Beausoleil SA, Villen J, Gerber SA, Rush J, Gygi SP. A probability-based approach for high-throughput protein phosphorylation analysis and site localization. Nat Biotechnol. 2006; 24:1285–1292. [PubMed: 16964243]
39. Trapnell C, et al. Differential gene and transcript expression analysis of RNA-seq experiments with TopHat and Cufflinks. Nat Protoc. 2012; 7:562–578. [PubMed: 22383036]

40. Anders S, Pyl PT, Huber W. HTSeq--a Python framework to work with high-throughput sequencing data. Bioinformatics. 2015; 31:166–169. [PubMed: 25260700]

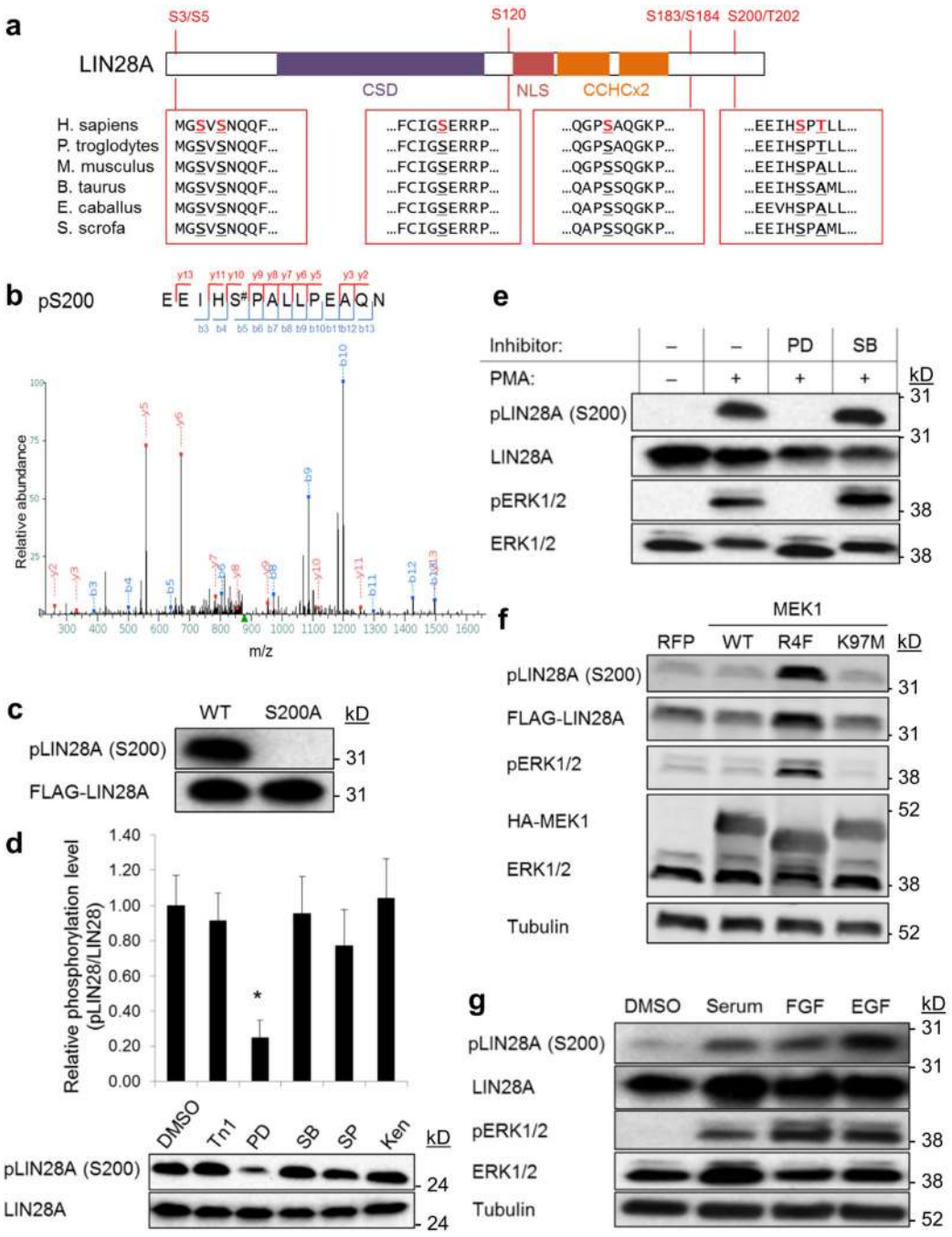

Figure 1. MAPK/ERK phosphorylates LIN28A on S200

(a) Schematic of the LIN28A domain structure with indicated phosphorylation sites, as mapped by mass spectrometry. Respective motifs and homologous sequences across several mammalian species are shown below each site. CSD = cold-shock domain; NLS = nuclear localization signal; CCHC = zinc finger domains.

(b) Representative phosphopeptide MS/MS spectrum for S200.

(c) Western blot analysis of LIN28A (S200) phosphorylation in HeLa cells stably expressing wild-type (WT) or phospho-null (S200A) FLAG-LIN28A. A representative image of three independent experiments is shown.
(d) Western blot analysis of LIN28A (S200) phosphorylation in PA1 hECCs after 60-min treatment with a panel of inhibitors of proline-directed kinases. Tn1 = Torin1 (100 nM); PD = PD0325901 (1 μM); SB = SB203580 (2 μM); SP = SP600125 (20 μM); Ken = Kenpaullone (5 μM). Quantification of Western blot data is shown on top. n=3 independent experiments. Error bars represent s.e.m. *P < 0.05 (two-tailed Student's *t*-test).
(e) Western blot analysis of LIN28A (S200) phosphorylation in PA1 cells after 30-min pre-treatment with DMSO, PD0325901 (1 μM), or SB203580 (2 μM), followed by 30-min treatment with DMSO or PMA (200 nM). Cells were serum-starved for 16–20 h prior to addition of inhibitors. A representative image of two independent experiments is shown.
(f) Western blot analysis of LIN28A (S200) phosphorylation in 293T cells stably expressing wild-type FLAG-LIN28A after transfection with RFP, wild-type (WT), constitutively active (R4F), or kinase-dead (K97M) MEK1. Cells were transfected, incubated for 48 h, and then serum-starved for 16–20 h prior to analysis. A representative image of two independent experiments is shown.
(g) Western blot analysis of LIN28A (S200) phosphorylation in PA1 cells after 30-min stimulation with serum (10%), fibroblast growth factor (FGF) (100 ng/ul), or epidermal growth factor (EGF) (100 ng/ul). Cells were serum-starved for 16–20 h prior to stimulation. A representative image of two independent experiments is shown. Statistics source data are shown in Supplementary Table 4. Unprocessed scans of blots are shown in Supplementary Fig. 5.

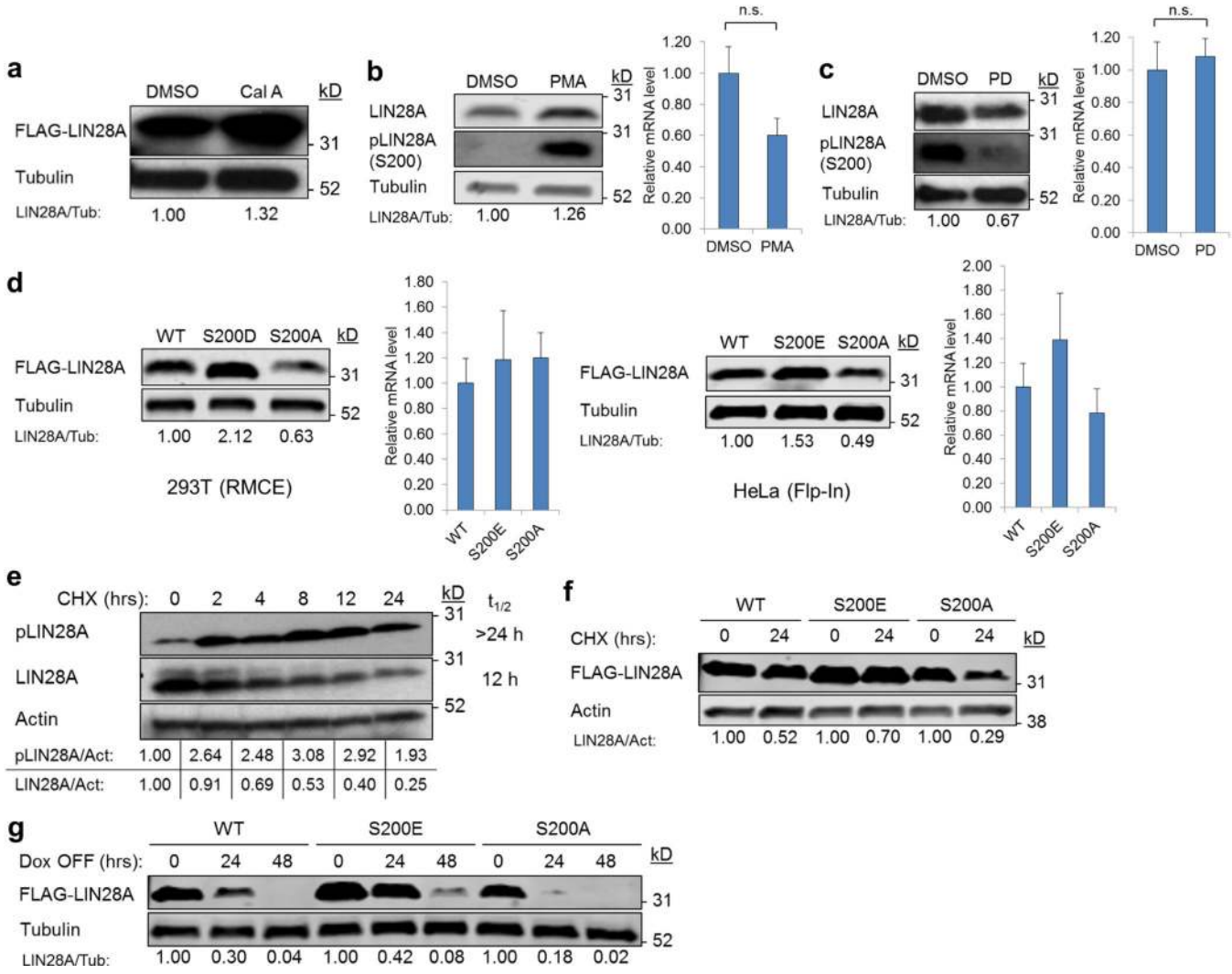

Figure 2. LIN28A phosphorylation increases its protein stability

(a) Western blot analysis of transgenic FLAG-LIN28A in iLIN28A mESCs after 30-min treatment with DMSO or Calyculin A (100 nM). A representative image of three independent experiments is shown.

(b) Western blot (left) and qRT-PCR (right) analysis of endogenous LIN28A in PA1 cells after three-hour treatment with DMSO or PMA (200 nM). Cells were serum-starved for 16–20 h prior to addition of drugs. n=3 independent experiments. Error bars represent s.e.m. n.s. = non-significant; P=0.09 (two-tailed Student's *t*-test).

(c) Western blot (left) and qRT-PCR (right) analysis of endogenous LIN28A in PA1 cells after 48-hour treatment with DMSO or PD0325901 (1 μM). n=3 independent experiments. Error bars represent s.e.m. n.s. = non-significant; P=0.79 (two-tailed Student's *t*-test).

(d) Western blot (left) and qRT-PCR (right) analysis of transgenic FLAG-LIN28A in isogenic 293T (RMCE) or HeLa (Flp-In) cells. Cells were engineered to stably express a single copy of the respective LIN28A variant: wild-type (WT), phospho-mimetic (S200D or S200E), or phospho-null (S200A). n=3 independent experiments. Error bars represent s.e.m.

P=0.77 (S200D) and P=0.70 (S200A) for 293T; P=0.42 (S200E) and P=0.48 (S200A) for HeLa (two-tailed Student's *t*-test).

(e) Cycloheximide chase of endogenous phospho- and total LIN28A in PA1 cells. CHX = cycloheximide (100 μg/ml). A representative image of two independent experiments is shown.

(f) Cycloheximide chase of transgenic FLAG-LIN28A variants in HeLa (Flp-In) cells. CHX = cycloheximide (100 μg/ml). A representative image of two independent experiments is shown.

(g) Chase of transgenic FLAG-LIN28A variants after Dox withdrawal (Dox OFF) in HeLa (Flp-In) cells. Dox = doxycycline (100 ng/ml). A representative image of two independent experiments is shown. Statistics source data are shown in Supplementary Table 4. Unprocessed scans of blots are shown in Supplementary Fig. 5.

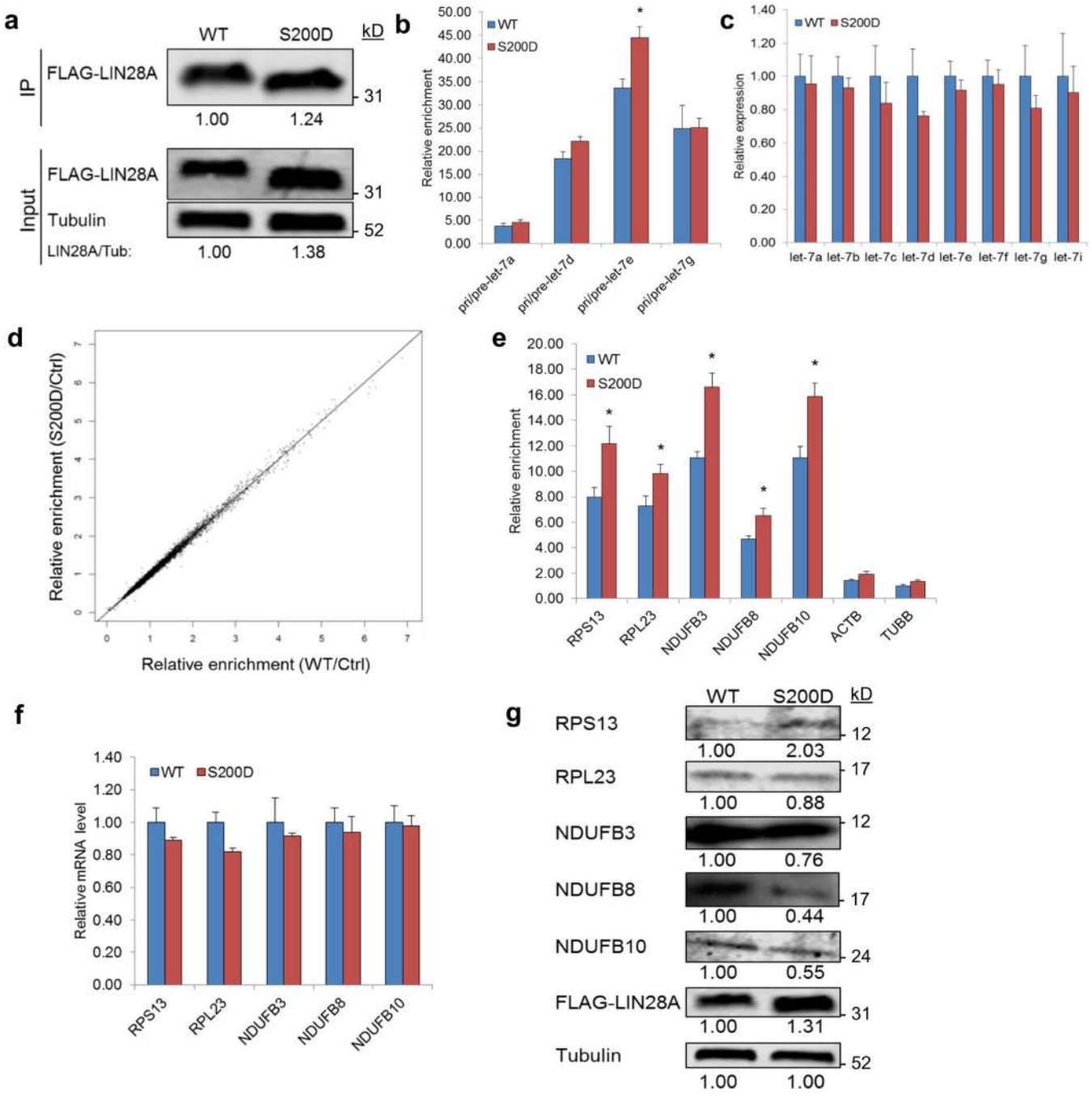

Figure 3. LIN28A phosphorylation can uncouple its *let-7*-dependent and independent activities

(a) Western blot analysis of RNA immunoprecipitation in PA1 cells overexpressing wild-type (WT) or phospho-mimetic (S200D) FLAG-LIN28A. A representative image of four independent experiments is shown.

(b) qRT-PCR analysis of pri/pre-*let-7* species immunoprecipitated by wild-type (WT) or phospho-mimetic (S200D) FLAG-LIN28A in PA1 cells. n=4 independent experiments. Data were normalized to cell number prior to RT. Error bars represent s.e.m. *P<0.05 (two-tailed Student's *t*-test, S200D vs. WT).

(c) qRT-PCR analysis of mature *let-7* species in PA1 cells stably overexpressing wild-type (WT) or phospho-mimetic (S200D) FLAG-LIN28A. n=3 independent experiments. Error bars represent s.e.m. P>0.05 (two-tailed Student's *t*-test, S200D vs. WT).
(d) RNA-seq analysis of mRNAs immunoprecipitated by wild-type (WT) or phospho-mimetic (S200D) FLAG-LIN28A in PA1 cells. Each dot represents an average enrichment value for transcripts from a given gene. n=3 independent experiments. Data were normalized to the amount of immunoprecipitated LIN28A prior to sequencing. Detailed description of the analysis is provided in the Methods section and the complete data set is available in Supplementary Table 2.
(e) qRT-PCR analysis of representative mRNA targets immunoprecipitated by wild-type (WT) or phospho-mimetic (S200D) FLAG-LIN28A in PA1 cells. n=4 independent experiments. Data were normalized to cell number prior to RT. Error bars represent s.e.m. *P<0.05 (two-tailed Student's *t*-test, S200D vs. WT).
(f) qRT-PCR analysis of representative mRNA targets in PA1 cells stably expressing wild-type (WT) or phospho-mimetic (S200D) FLAG-LIN28A. n=3 independent experiments. Error bars represent s.e.m. P>0.05 (two-tailed Student's *t*-test, S200D vs. WT).
(g) Western blot analysis of representative mRNA targets in PA1 cells stably expressing wild-type (WT) or phospho-mimetic (S200D) FLAG-LIN28A. A representative image of three independent experiments is shown. Statistics source data are shown in Supplementary Table 4. Unprocessed scans of blots are shown in Supplementary Fig. 5.

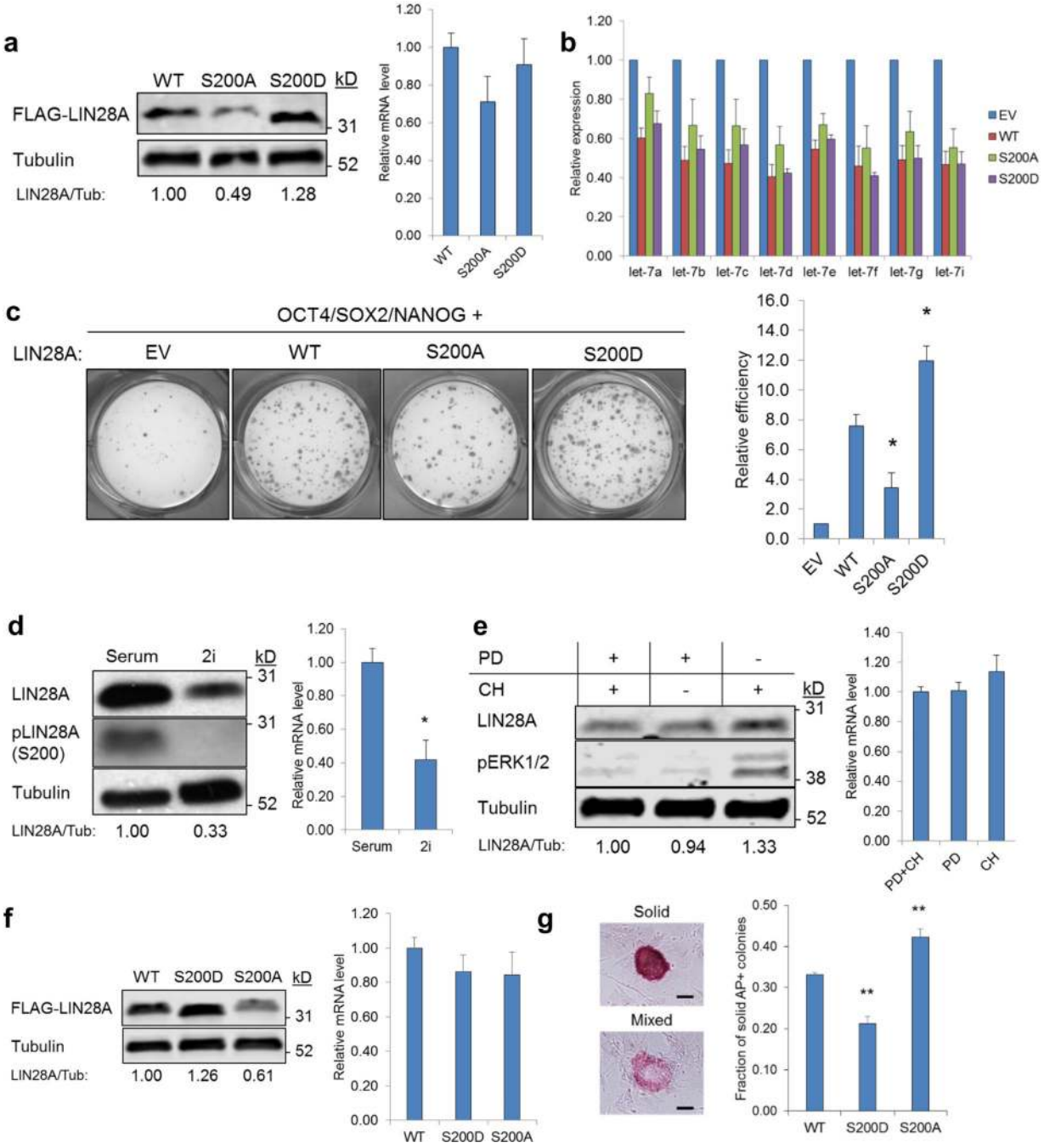

Figure 4. LIN28A phosphorylation contributes to the regulation of pluripotency transitions

(a) Western blot (left) and qRT-PCR (right) analysis of wild-type (WT), phospho-null (S200A), and phospho-mimetic (S200D) FLAG-LIN28A at day 6 of reprogramming. n=4 independent experiments. Error bars represent s.e.m. P=0.10 (S200A) and P=0.52 (S200D) (two-tailed Student's *t*-test vs. WT).

(b) Levels of mature *let-7*s at day 6 of reprogramming using respective LIN28A constructs. EV = empty vector. n=4 independent experiments. Error bars represent s.e.m. P>0.05 (two-tailed Student's *t*-test vs. WT).

(c) TRA-1-60 staining of iPSCs harboring empty vector (EV), wild-type (WT), phospho-null (S200A), or phospho-mimetic (S200D) FLAG-LIN28A (day 21 of reprogramming). Quantification of reprogramming efficiency based on the number of TRA-1-60$^+$ colonies is shown on the right. n=4 independent experiments. Error bars represent s.e.m. *P<0.05 (two-tailed Student's *t*-test vs. WT).

(d) Western blot (left) and qRT-PCR (right) analysis of endogenous LIN28A in v6.5 mESCs cultured in serum/LIF or 2i/LIF. n=3 independent experiments. Error bars represent s.e.m. *P<0.05 (two-tailed Student's *t*-test).

(e) Western blot (left) and qRT-PCR (right) analysis of endogenous LIN28A in v6.5 mESCs after a four-hour dropout of PD0325901 (PD) or CHIR99021 (CH). n=3 independent experiments. Error bars represent s.e.m. P=0.99 (PD) and P=0.89 (CH) (two-tailed Student's *t*-test vs. PD+CH).

(f) Western blot (left) and qRT-PCR (right) analysis of transgenic wild-type (WT), phospho-mimetic (S200D), or phospho-null (S200A) FLAG-LIN28A added back in LIN28A/B KO mESCs. n=3 independent experiments. Error bars represent s.e.m. P=0.63 (S200D) and P=0.60 (S200A) (two-tailed Student's *t*-test vs. WT).

(g) Alkaline Phosphatase (AP) analysis of mESCs from panel (f) grown at clonal density upon transfer from 2i/LIF to serum/LIF. Representative images of colonies with solid and mixed staining patterns are shown on the left. Scale bar = 100 μm. Quantification of the fraction of solid colonies is shown on the right. n=4 independent experiments. Error bars represent s.e.m. **P<0.01 (two-tailed Student's *t*-test). Statistics source data are shown in Supplementary Table 4. Unprocessed scans of blots are shown in Supplementary Fig. 5.